Life Sciences 290 (2022) 120247

Contents lists available at ScienceDirect

Life Sciences

journal homepage: www.elsevier.com/locate/lifescie

A novel assay to assess the effects of estrogen on the cardiac calmodulin binding equilibrium

Kyle Kaster [1,2], John Patton [1,3], Sarah Clayton, Eric Wauson, Jennifer Giles, Quang-Kim Tran [*]

Department of Physiology & Pharmacology, Des Moines University Osteopathic Medical Center, IA 50312, United States

ARTICLE INFO

Keywords:
Menopause
Estrogen
Heart
Calmodulin
Calmodulin-binding proteins

ABSTRACT

Aims: The Ca^{2+}-binding protein calmodulin (CaM) modulates numerous target proteins but is produced insufficiently to bind all of them, generating a limiting CaM equilibrium. Menopause increases cardiac morbidity; however, it is unknown if the cardiac CaM equilibrium is affected by estrogen. We devised an assay to assess the effects of ovariectomy and estrogen treatment on the cardiac CaM equilibrium.

Materials and methods: Sprague-Dawley rats received sham surgery or ovariectomy, followed by 2-week treatment with vehicle or 17β-estradiol. Ca^{2+}-saturated left ventricular (LV) lysates were processed through CaM sepharose columns, which retained CaM-binding proteins unoccupied by endogenous CaM. Eluants therefrom were subjected to a competitive binding assay against purified CaM and a CaM biosensor to assess the amounts of unoccupied CaM-binding sites. LV cellular composition was assessed by immunohistochemistry.

Key findings: LV eluants processed from sham animals reduce biosensor response by ~32%, indicating baseline presence of unoccupied CaM-binding sites and a limiting CaM equilibrium. Ovariectomy exacerbates the limiting CaM equilibrium, reducing biosensor response by ~65%. 17β-estradiol treatment equalizes the difference between sham and ovariectomized animals. These changes reflect whole tissue responses and are not mirrored by changes in total surface areas of cardiomyocytes and fibroblasts. Consistently, Ca^{2+}-dependent, but not Ca^{2+}-independent, interaction between CaM and the cardiac inositol trisphosphate receptor (IP_3R) is reduced following ovariectomy and is restored by subsequent 17β-estradiol treatment.

Significance: Our assay provides a new parameter to assess tissue CaM equilibrium. The exacerbated limiting CaM equilibrium following estrogen loss may contribute to cardiac morbidity and is prevented by estrogen treatment.

1. Introduction

Calmodulin (CaM) is a Ca^{2+}-binding protein that plays a critical role in signal transduction across tissues. Evolutionarily, this is evidenced by the fact that CaM is encoded by three genes (*CALM1, CALM2* and *CALM3*). CaM is composed of two globular domains (lobes) linked together by a flexible central helix. Each CaM lobe contains two Ca^{2+}-binding sites. Upon production of an intracellular Ca^{2+} signal, Ca^{2+}-CaM complexes interact with numerous target proteins and modify their activities [1]. CaM can also interact with some proteins in a Ca^{2+}-independent fashion [2]. In the heart, CaM plays crucial roles in organ development, systolic and diastolic functions, and regulation of cardiac rhythm. CaM-binding proteins (CBPs) such as CaM kinases are important for many cardiac functions and myocardial cell survival programs [3]. Mutations in CaM genes are associated with abnormal repolarization and myocardial sensitivity to β adrenergic stimulation and deadly catecholaminergic polymorphic ventricular tachycardia [4,5].

It has been estimated that CaM can interact with a network of over 300 CBPs [6]. Despite this universal requirement, the availability of CaM is insufficient for its target proteins. Indeed, up to 60% of CaM in mammalian tissues is tied up by inseparable associations that render it unavailable for dynamic binding with other target proteins [7]. Studies in endothelial cells indicated that insufficient CaM level generates competition among CaM target proteins [8,9]. This limiting CaM equilibrium has also been noted in smooth muscle cells [10], human

* Corresponding author.
E-mail address: kim.tran@dmu.edu (Q.-K. Tran).
[1] Current addresses: Department of Orthopedic Surgery, Michigan State University, McLaren Greater Lansing, MI, United States.
[2] These authors contributed equally to this work.
[3] Department of Pediatrics, University of Texas Health Science Center at Houston, TX, United States.

https://doi.org/10.1016/j.lfs.2021.120247
Received 4 October 2021; Received in revised form 8 December 2021; Accepted 14 December 2021
Available online 23 December 2021

embryonic kidney 293 cells [11] and neurons [12]. In cardiomyocytes, only ~2% of total CaM is freely available [13]. Thus, conditions that alter the relationship between CaM and its target proteins likely have extensive effects on cardiovascular functions.

Menopause is associated with significant increases in the risk and incidence of cardiovascular diseases. This has been attributed to the reduction in circulating estrogen [14,15]. Nevertheless, it is entirely unknown how menopause and estrogen replacement affect the network of CaM-binding proteins in the heart. We have previously shown that in the vascular endothelium, 17β-estradiol upregulates CaM level via a feed-forward mechanism that involves activation of the G protein-coupled estrogen receptor (GPER) leading to transactivation of EGFR and MEK1 [16]; this is associated with ~8-fold increase in free Ca^{2+}-liganded CaM in response to a generic Ca^{2+} signal and significant increases in the association between CaM and several CBPs of disparate affinities for CaM, including eNOS, plasma membrane Ca^{2+}-ATPase4b, estrogen receptor α and GPER itself. However, because of the multitude of CaM targets and the complexities of interactions among them and CaM, the impact of an altered physiological or pathological condition and a therapeutic intervention on the CaM network cannot be fully assessed without consideration of changes in the pool of CBPs that need but do not have access to CaM.

In this work, we have devised an approach to assess this pool of CBPs in the heart and utilized it to examine the effects of ovariectomy and estrogen treatment.

2. Methods and materials

2.1. Animals/animal care

Nine-week-old female Sprague-Dawley rats were purchased from Charles River Laboratories (Wilmington, MA) and housed in temperature- (22 ± 0.2 °C) and light- (12/12-h dark/light) controlled animal quarters. The rats were adapted to the laboratory for at least 7 days before experimentation. They had free access to rat chow (7013 NIH-31 modified rat diet, 0.25% NaCl) and drinking water. All experiments were conducted in accordance with the National Institutes of Health recommendation to follow the Guide for the Care and Use of Laboratory Animals of the National Research Council of the (U.S.) National Academies and were approved by Des Moines University Institutional Animal Care and Use Committee.

2.2. In-vivo experimental overview

Four groups of animals (n = 8–10 each, average body weight 175 ± 2.7 g) were used in the study. Two groups received sham surgery and the other two received ovariectomy (OVX). Subgroups of sham and OVX animals received exogenous estrogen for two weeks via osmotic pumps, which were implanted during the OVX or sham surgery, ensuring estrogen levels were never depleted. The remaining groups served as time controls. At the end of the experimental timeline, the animals were euthanized with carbon dioxide and tissues were harvested and immediately flash-frozen with liquid nitrogen.

2.3. Surgical procedures

Ovariectomy: under isoflurane anesthesia, each ovary was isolated through the abdominal wall, tied off with sterile suture, and removed. The incision was then closed with suture, and the procedure was repeated on the contralateral side. The skin was closed with surgical staples. In sham surgeries, the ovary was isolated but not removed. Osmotic minipumps (Model 2002; Alzet, Cupertino, CA) were implanted subcutaneously during the same OVX or sham surgery to deliver 17β-estradiol (30 μg/day) continuously for 2 weeks. Considering the average body weight of 175 g, this dose was predicted to produce a serum concentration within the physiological concentration range in rats, based on previously published similar doses and serum measurements [17,18]. A single 3-cm dorsal midline incision was made in the skin and underlying muscles. The pumps were then implanted subcutaneously in the backs of the animals. The skin was closed with surgical staples.

2.4. Preparation of left ventricular samples

After animal euthanasia, left ventricles (LV) were isolated from hearts by removing the atria and right ventricles. After removal of any residual blood clots within LV chambers using physiological saline solution, LV tissues were minced and then lysed in lysis buffer (in mM: 25 Tris-HCl, 148 NaCl, 97.6 NaF, 27.8 $Na_4P_2O_7$, 271.8 Na_3VO_4, Triton X-100 (1% vol/vol), trypsin inhibitor (45 μM), 1:200 protease inhibitor cocktail (Sigma) and 2 μg/mL PMSF, containing 1 mM $CaCl_2$) and shaken with 2-mm glass beads in a bead beater at 4 °C for 10 min. Samples were then centrifuged at 21,000 ×g for 10 min at 4 °C. The supernatant was collected, and protein concentrations were determined in triplicate using the Pierce BCA protein assay kit (Thermo Fisher Scientific, Rockford, IL). CaM sepharose 4B was washed three times in binding buffer (in mM: 25 Tris-HCl, 100 NaCl, 1 $CaCl_2$, pH 7.4) Samples containing 650 μg total protein each were then mixed with 100 μL of CaM Sepharose 4B (GE Healthcare), adjusted by binding buffer to a total volume of 1.5 mL and gently rocked at 4 °C for 1 h. After spinning at 1000 ×g, the supernatant was separated, and CaM-binding proteins that were unoccupied by endogenous CaM (*uo*CBPs) and now bound to the CaM Sepharose were washed three times in binding buffer. Bound proteins were eluted by rocking the sepharose in 600 μL of elution buffer (in mM: 25 Tris-HCl, 100 KCl, 3 EGTA, pH 7.4) for 45 min at 4 °C. Subsequently, eluants were subjected to multiple rounds of buffer exchange at 4 °C using 3000 MWCO Centriprep centrifugal filters (EMD Millipore) in equal volumes of titration buffer (in mM: 25 Tris-HCl, 100 KCl, pH 7.4) to achieve a final EGTA concentration <1 μM and a final volume of 600 μL. Final eluants were immediately used in competitive binding assays.

2.5. Competitive binding assay to determine unsaturated CaM-binding sites in LV tissue

CaM and the $BSCaM_{45}$ biosensor were purified as described previously [19]. To measure the relative amounts of unoccupied CaM-binding sites in the left ventricle after each treatment, CaM was titrated into a quartz cuvette (Hellma Analytics USA, Plainview, NY) containing a 600-μL mixture of 50 nM $BSCaM_{45}$, 0.1 mg/mL BSA, 25 mM Tris, 100 mM KCl,1 mM Ca^{2+} including 530 μL of LV eluant or molecular grade water. $BSCaM_{45}$ was excited at 430 nm while its emission was collected between 460 and 560 nm using a QuantaMaster™40 (Photon Technologies International, Brattleboro, VT). Fractional biosensor response in the absence of LV eluant (FR_0) was determined by the formula

$$FR_0 = (R - R_{min})/(R_{max} - R_{min}) \quad (1)$$

where R_{min} and R_{max} are the ratios between emission intensities at 475 and 530 nm in the absence of CaM or presence of saturating CaM, respectively. Biosensor responses in the presence of LV eluants (FR_{LV}) were subsequently obtained and expressed as relative values compared to the response in the absence of LV eluants at each concentration of CaM. The relative percent unoccupied CaM-binding sites (*uo*CBPs) in each eluant was calculated by the formula

$$uoCBPs = 100 \times (FR_0 - FR_{LV})/FR_0 \quad (2)$$

where FR_0 was the biosensor fractional ratio obtained in the absence of LV eluant.

2.6. Immunohistochemistry (IHC) of LV sections

Following euthanasia of the animals, the right ventricles and atria were excised from the left ventricles. The LV chambers were then

excised along their longitudinal axes through the anterior and posterior walls, followed by removal of residual blood clots with normal saline. The left halves of the LV sections, including parts of the anterior and posterior walls and the entire left lateral walls, were placed face up in plastic molds containing optimized cutting temperature solution (OCT) and frozen in −80 °C. Frozen LVs were then sliced longitudinally using a Leica CMs 1850 cryostat into 5-μm sections, which were adsorbed onto glass slides and kept frozen until IHC staining. LV slices were next fixed in 4% paraformaldehyde for 15 min at room temperature and permeabilized by incubating in 0.25% Triton X-100 in phosphate buffered saline (PBS) for 15 min. After several washes, the samples were blocked in 10% goat serum in PBS for 1 h at room temperature. Blocking solution was then removed and the samples were incubated overnight at 4 °C in a humidifying chamber with a mouse monoclonal anti-troponin T antibody (ThermoFisher Cat.# ms-295-P1) and a rabbit monoclonal anti-vimentin antibody (Cell Signaling, Cat.# 5741S), both at 1:200 dilution. A sample was exposed to no primary antibodies but secondary antibodies only for use as control. Slides were then washed 3–5 times in PBS containing 0.1% Tween 20, followed by applying AlexaFluor594 goat anti-mouse IgG (Invitrogen Cat.# A11032) and AlexaFluor488 goat anti-rabbit IgG (Invitrogen Cat.# A11034), both at 1:200 dilution. Slides were then incubated at room temperature for 1 h. One of the samples was not given secondary antibody (for detection of background autofluorescence). Slides were then washed in PBS containing 0.1% Tween for 3–5 min. DAPI Fluoromount-G (SouthernBiotech, Cat.# 0100-20) was applied before a coverslip was placed on top of the stained LV tissue. The edges of the coverslips were then sealed with transparent glue and samples allowed for cure at room temperature in the dark overnight. Fluorescence detection for DAPI, AlexaFluor488, and AlexaFluor594 was carried out using a Zeiss Axioskop trinocular upright microscope at the appropriate wavelengths. For each LV section, the base, middle region, and the apex were each imaged at two regions distributed evenly over the anterior and posterior walls, so that three main regions of LV tissues were imaged across samples. Image capture was performed using the QCapture Pro 7 software (Teledyne Photometrics), with equal capture parameters applied throughout regions of each section and across samples.

Total surface areas (TSA) of cardiomyocytes and fibroblasts were analyzed using NIH ImageJ software. Captured fluorescent images from all treatment conditions were exposed to identical threshold parameters and fluorescence wavelengths. These parameters were determined using the control samples in which only the secondary antibodies were applied in the IHC process, by adjusting until all background and autofluorescence were eliminated (yielding a measured area of zero). All cell zones were subsequently selected, and their surface areas were calculated using the measure function of ImageJ. Values of TSA across sampling windows in compatible regions were subjected to Grubbs test to remove outliers, followed by application of ANOVA for comparisons.

To determine the relative total surface areas of fibroblasts compared to cardiomyocytes, the peak emission intensities of equal concentrations of the secondary antibodies (1:200 dilution) were first compared in a QuantaMaster™40 spectrofluorometer (Photon Technologies International, Brattleboro, VT). AlexaFluor488 goat anti-rabbit IgG and AlexaFluor594 goat anti-mouse IgG were excited at λ488 and λ594 nm, respectively, while their emission intensities were scanned from λ495–600 nm and λ600–700 nm, respectively. The ratio of the peaks was then factored in the measured total areas of fibroblasts and cardiomyocytes to determine the ratio of their surface areas ($TSA_{CF/CM}$) across LV regions.

2.7. Coimmunoprecipitation and Western blotting

The following procedure was performed with or without 1 mM $CaCl_2$ in all solutions in all steps, from lysis to immunoblotting. Left ventricular tissues were isolated as described under “Preparation of LV tissues”. Following BCA, 3 mg of total protein from LV lysates was rocked with 2 μg mouse monoclonal anti-CaM antibody (EMD Millipore, Cat.# 05-173 MI). Samples were then mixed with equal volumes of protein A/G beads (Santa Cruz Biotech, Cat.# SC2003) and gently rocked for 2 h at 4 °C before centrifugation and elution of supernatant for immunoblotting. After SDS-PAGE, membranes were cut between the levels of inositol trisphosphate receptor (IP_3R, ~ 280 kDa) and the heavy chain (~50 kDa). After blocking, the upper fragments were incubated overnight with a knockout-verified rabbit monoclonal anti-IP_3R antibody (Abcam, Cat.# ab108517), while the lower fragments was incubated in blocking buffer containing no primary antibody. After washes, the upper fragment was incubated with VeriBlot IgG (ab131368) while the lower fragment was incubated with Peroxidase AffiniPure F(ab′)2 Fragment rabbit anti-mouse IgG (Jackson Immuno Research Labs, Cat.# 315,036,046). Total lysates (50 μg each) from samples were also immunoblotted for assessment of the inputs of total CaM. Following SDS-PAGE, membranes were briefly stained with Ponceau S (Fisher Scientific Cat.# BP103-10), followed by washes and incubation with the anti-CaM antibody. After development with enhanced chemiluminescence, densitometric capture and analyses were carried out using a ChemiDoc™ XRS+ imaging system and ImageLab 6.0 software package (Bio-Rad, Hercules, CA).

2.8. Statistical analysis

Data are expressed as means ± SD. Statistical analysis was performed using OriginPro 2020 software (OriginLab Corp., Northampton, MA). Statistical comparison was done using one-way ANOVA. Tukey post hoc test was applied where appropriate. Statistical significance was determined as $p < 0.05$.

3. Results

3.1. Principles of assay to assess unoccupied CaM-binding proteins in LV tissue

As the availability of CaM is limited in cardiac tissues [13,20], evaluation of the impact of an altered physiological or a pathological condition and therapeutic intervention on the cardiac CaM network would benefit from an ability to separate CaM-binding proteins (CBPs) that are occupied by endogenous CaM (*o*CBPs) and those that are unoccupied (*uo*CBPs). To do this, LV lysates from sham and ovariectomized (OVX) female rats treated with and without 17β-estradiol are first allowed to interact with CaM sepharose (Step (1), Fig. 1A). This step allows for *uo*CBPs to interact with and be retained by CaM sepharose. The appropriate amounts of lysates and sepharose to guarantee complete capture of *uo*CBPs are determined by competitive binding assays (described below) to show that no CaM-binding capacity remains in the flow-through. The *uo*CBPs are then eluted by chelating Ca^{2+} in the CBPs-Ca^{2+}-CaM sepharose complexes, which releases the CBPs (Step (2), Fig. 1A). Following multiple rounds of buffer exchange to essentially eliminate the Ca^{2+} chelator (Step 3, Fig. 1A), the relative amounts of *uo*CBPs are assessed by a competitive binding assay using purified CaM and a CaM biosensor in the presence of saturating Ca^{2+} concentration (Fig. 1B). In this assay, the CaM biosensor is composed of a FRET pair of fluorescent proteins (ECFP-EYFP) flanking the CaM-binding domain of myosin light chain kinase. Many CaM biosensors of similar format with different insert sequences have been generated and characterized for various purposes [19,21–25]. The biosensor $BSCaM_{45}$ chosen in this study has been characterized and used in several cell types, including cardiomyocytes, to measure free Ca^{2+}-liganded CaM with high sensitivity and specificity [20,22,26]. Herein, it is used not to measure free Ca^{2+}-CaM levels, but to report the amount of prebound Ca^{2+}-CaM leaving for *uo*CBPs from left ventricular tissues. CaM is incrementally added to interact with the biosensor in the presence of saturating Ca^{2+} concentration as biosensor responses are monitored. This disrupts FRET between the donor ECFP and acceptor EYFP (left panel, Fig. 1B). In the

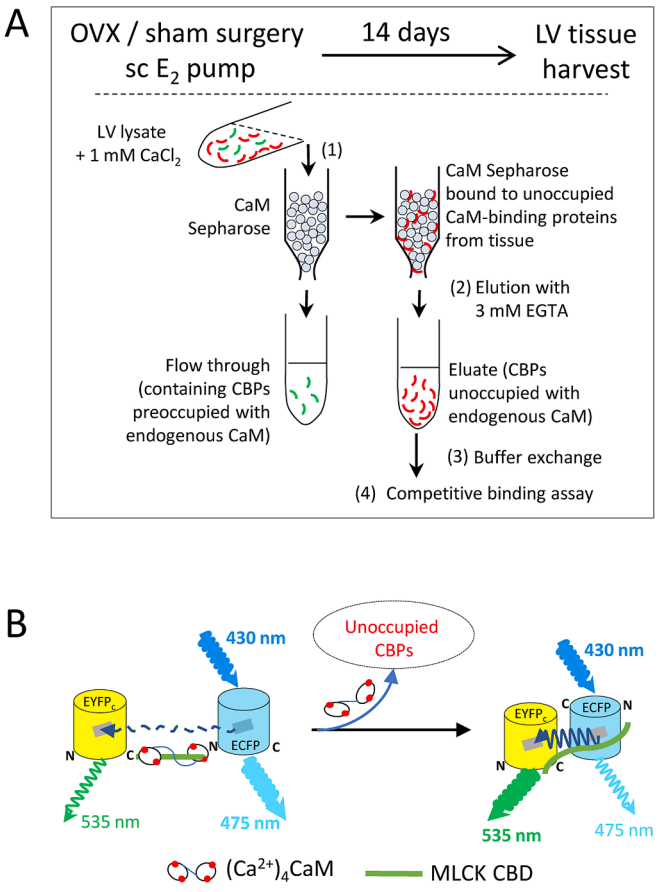

Fig. 1. Assay outline to assess cardiac CaM binding equilibrium. A) Experiment timeline and main steps of assay (see text for detailed description). Green curves in solution, occupied CaM-binding proteins; red curves in solution, unoccupied CaM-binding proteins. B) Principle of competitive binding assay using purified CaM and CaM biosensor to assess eluants from Step (3) in (A). $(Ca^{2+})_4$-CaM, Ca^{2+}-saturated CaM; MLCK, myosin light chain kinase; CBD, CaM-binding domain. ECFP, enhanced cyan fluorescent protein; EYFPc, "citrine" enhanced yellow fluorescent protein; CBPs, CaM-binding proteins. (For interpretation of the references to colour in this figure legend, the reader is referred to the web version of this article.)

presence of LV eluate that contains *uo*CBPs, CaM titrated into the mixture will be competed for by these proteins and the biosensor, resulting in reduction in biosensor response (right panel, Fig. 1B). Comparisons between biosensor responses in the absence and presence of LV eluates allow for an assessment in the shortage of CaM in LV tissue in normal, disease and treated conditions.

3.2. Animal body weight, tool verification and assay conditioning

Animal body weights are presented in Fig. 2A. Ovariectomized rats gained significantly more weight than sham animals. 17β-estradiol treatment significantly prevented the gain in body weight in both sham animals and ovariectomized animals. Preparations of purified biosensors and CaM were run on Coomassie gel, showing undegraded, single bands at expected sizes (Fig. 2B). In vitro titration of CaM into biosensor mixture in the presence of saturating Ca^{2+} concentration demonstrated a classic behavior of FRET disruption upon increasing CaM concentration, with reciprocal increases in 475 nm emission intensity and decreases in 530 nm emission intensity (Fig. 2C). Plot of the biosensor response against CaM concentration yielded an apparent K_d value of 44 ± 1.7 nM, consistent with reported value [22] (Fig. 2D, black circles). To determine the appropriate amounts of LV lysate and CaM sepharose in Step (1), Fig. 1A, various ratios of LV eluate and CaM

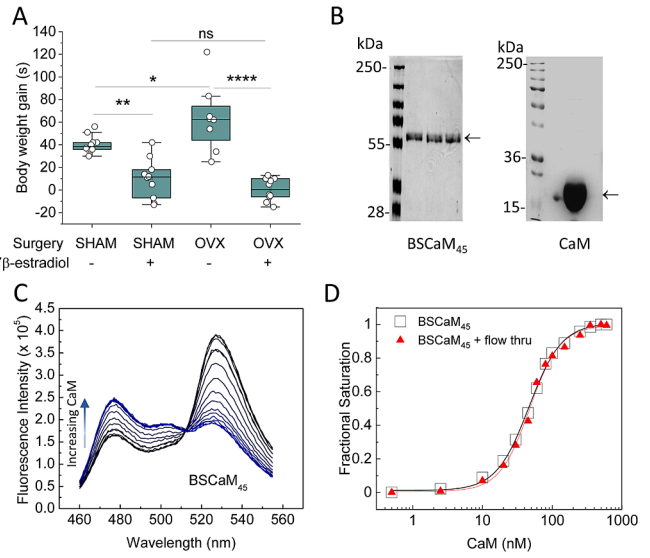

Fig. 2. Animal body weight data and assay conditioning. A) Body weight gains across experimental groups. B) Coomassie stains of purified biosensor and CaM preparations. C) Spectral change of biosensor in response to CaM titration. D) Biosensor fractional saturation as a function of CaM in the absence (open squares) or presence (closed triangles) of 530 μL of flow-through from Step 1, Fig. 1A. Total assay volume, biosensor, Ca^{2+} and CaM concentration were identical in the two conditions. *, $p < 0.05$; **, $p < 0.01$; ****, $p < 0.0001$. Data are means ± SD from $n = 8$–10 animals for A; $n = 3$ for each condition in D.

sepharose were tested to reach a condition in which flow-through in this step did not produce any competitive effect on biosensor response, guaranteeing that all *uo*CBPs had been retained by CaM sepharose. Fig. 2D (red triangles) shows a CaM titration curve in the presence of 530 μL of supernatant from mixing of 650 μg LV lysate from OVX animals and 100 μL of CaM sepharose (described in Step (1), Fig. 1A. see Methods for assay details). No reduction in biosensor response was observed compared to titrations in the absence of LV eluant, indicating all unoccupied CaM-binding sites had been bound to the CaM sepharose. These parameters were obtained through tests with LV eluants from all four groups of animals. In the absence of CaM, the presence of LV eluates did not alter biosensor response (not shown).

3.3. Effects of ovariectomy and 17β-estradiol treatment on the CaM binding equilibrium in LV tissue

To assess the effects of the loss of ovarian hormones and estrogen treatment on the cardiac CaM binding equilibrium, relative *uo*CBPs were assessed in LV tissues from animals receiving sham or OVX surgeries with and without treatment with 17β-estradiol. Fig. 3A shows $BSCaM_{45}$ fractional response to CaM titration in the absence or presence of LV eluants that had been processed through Step (3), Fig. 1A. The presence of LV eluants from all conditions resulted in a downward and rightward shift in the binding curve, indicating presence of *uo*CBPs.

To quantitatively compare the changes in *uo*CBPs across conditions, relative *uo*CBPs were compared at CaM concentrations corresponding to 25%, 50% and 75% fractional responses of the biosensor in the absence of LV lysate (FR_0). As predicted based on the widespread limiting CaM conditions across tissues [7–10,12,13,20], LV eluants from sham animals presented a ~32% *uo*CBPs compared to FR_0 at all three FR_0 levels (Fig. 3B). Strikingly, LV eluant from OVX animals resulted in a significant increase in *uo*CBPs to a ~65% value. In sham animals, treatment with 17β-estradiol increased LV *uo*CBPs slightly. Notably, early estrogen replacement abolished the difference between *uo*CBPs in LV eluants from sham and ovariectomized animals (Fig. 3B). No statistical differences were observed between *uo*CBPs values obtained at 25%, 50% or 75% of FR_0 in each group, indicating good sensitivity range of the

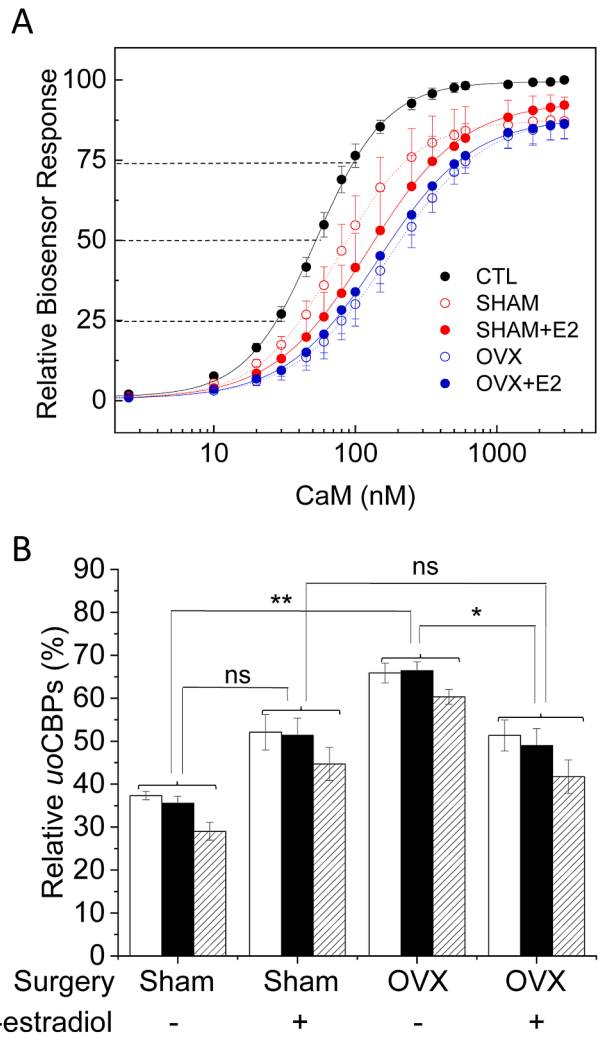

Fig. 3. Effect of experimental menopause and estrogen replacement on unoccupied CaM-binding proteins in LV tissue. A) Relative $BSCaM_{45}$ responses to CaM titration in the absence (CTL, closed circles) or presence of 530 μL eluants (Step 3, Fig. 1A) from equal protein contents (Step 1, Fig 1A) of LV lysates from sham or OVX animal treated with 17β-estradiol (E_2) for 2 weeks. Total assay volume, biosensor, Ca^{2+} and CaM concentration were identical across the groups. B) Relative unoccupied CaM-binding proteins (*uo*CBPs) calculated from biosensor responses in A at corresponding 25% (open columns), 50% (filled columns) and 75% (hatched columns) of control biosensor responses (dashed lines in A). *, $p < 0.05$; *, $p < 0.01$; ns, non-significant. Data are means ± SD from $n = 5$ repetitions for each condition.

biosensor response.

3.4. *Effects of ovariectomy and 17β-estradiol treatment on total surface areas (TSA) of cardiomyocytes and fibroblasts*

To assess if the observed changes in *uo*CBPs could be caused by changes in cellular compositions as a result of OVX and/or 17β-estradiol treatment, we performed immunohistochemistry for cardiomyocytes, using troponin T (TnT), and cardiac fibroblasts, using vimentin (Vim), from sections of LV chambers from animals exposed to these procedures and treatment. Cardiomyocytes occupy up to 80% volume of the rat heart [27] and are thus expected to contribute the most to the *uo*CBPs in our CaM equilibrium assay. Cardiac fibroblasts occupy only about 1.8% volume of the rat heart [27] and are not expected to contribute significantly to the *uo*CBPs in our assay. However, these cells are the main non-myocyte cell type [28,29]. Fig. 4A depicts the IHC sampling

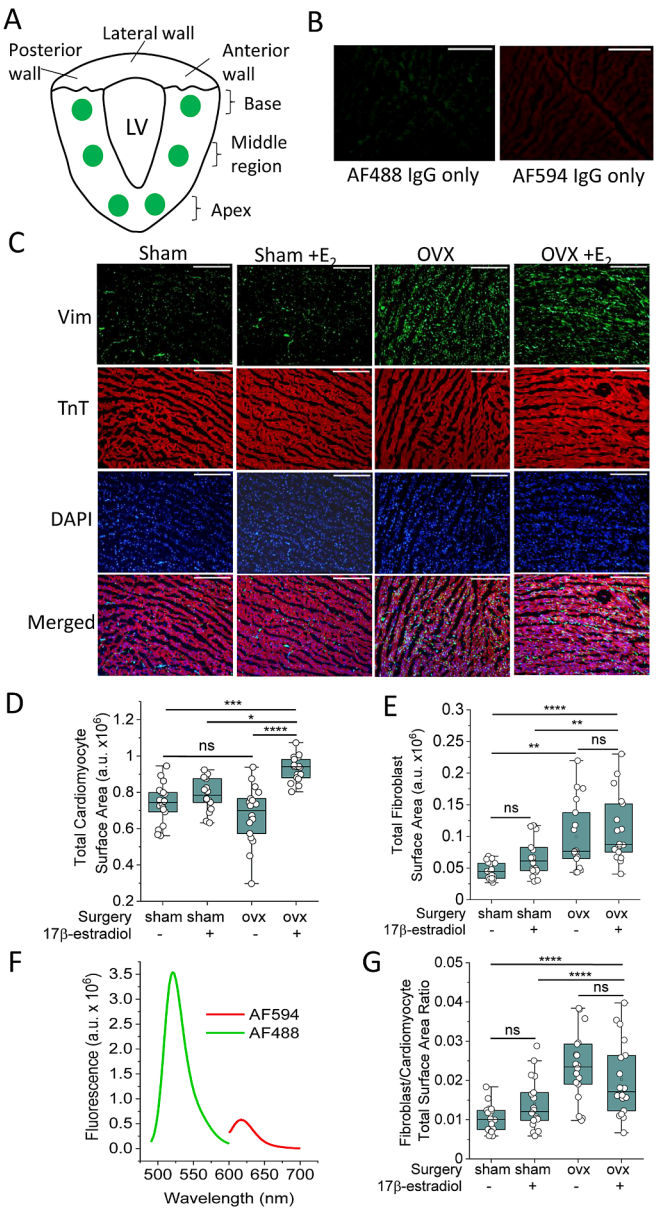

Fig. 4. Immunohistochemistry of LV tissues for cardiomyocytes and fibroblasts. Following OVX and/or 17β-estradiol treatment, LV tissue preparation and sectioning were carried out as described in the Methods section. A) Diagram of LV sectioning and imaging locations in each section. B) Control images of LV sections processed though IHC procedures with only fluorescent secondary antibodies, AlexaFluor488 goat anti-rabbit IgG (left) and AlexaFluor594 goat anti-mouse IgG (right), but without primary antibodies. C) Background-subtracted IHC images for vimentin (Vim), troponin T (TnT), nuclei (DAPI) and merged of these. D) Total surface area of cardiomyocytes. E) Total surface area of cardiac fibroblasts. F) Emission spectra and peaks of equal concentration (1:200 dilution) AlexaFluor 488 goat anti-rabbit IgG (green) and AlexaFluor 594 goat anti-mouse IgG (red). G) Relative total surface areas between fibroblasts and cardiomyocytes in the same LV sections ($TSA_{CF/CM}$). See text for description. Data are means ± SD from 6 sampling windows (depicted in A) in each LV section, $n = 3$ animals from each treatment condition. ns, non-significant; *, $p < 0.05$; **, $p < 0.01$; ****, $p < 0.0001$; scale bars, 200 μm. (For interpretation of the references to colour in this figure legend, the reader is referred to the web version of this article.)

strategy. Both the anterior and posterior wall sections of the base, middle region, and apex were sampled to provide a general assessment of various regions of the LV chamber. For the cardiomyocytes, ovariectomy did not affect TSA; however, 17β-estradiol treatment in OVX

animals caused a significant increase in myocardial TSA, compared to both untreated OVX and untreated sham animals (Fig. 4C-D). Interestingly, for the fibroblasts, OVX caused a significant increase in their TSA, and 17β-estradiol treatment did not reduce this effect (Fig. 4C and E).

To compare the degree of changes in surface areas between cardiac fibroblasts and cardiomyocytes ($TSA_{CF/CM}$) and effects of OVX and/or 17β-estradiol treatment on this ratio, we first compared the emission intensities of equal concentrations of the fluorescent antibodies used for troponin T (cardiomyocytes) and vimentin (fibroblasts). Since ImageJ measures TSA based on the detected intensities of the secondary antibodies, this ratio was used to correct for the ratio between measured TSA values for the fibroblasts (Fig. 4E) and cardiomyocytes (Fig. 4D). Equal concentrations (1:200 dilution) of AlexaFluor 488 goat anti-rabbit IgG and AlexaFluor 594 goat anti-mouse IgG were exposed to their respective excitation wavelengths with equal spectrofluorometric setups, and their respective emission spectra scanned as described in the Methods section. The corresponding peak emission intensities at λ525 nm and λ620 nm were 3.5×10^6 and 0.57×10^6, respectively, yielding an intensity ratio of 6.14 (Fig. 4F). Factoring this difference into the measured TSAs for fibroblasts (Fig. 4E) and cardiomyocytes (Fig. 4D), estimates of the relative TSAs between fibroblasts and cardiomyocytes ($TSA_{CF/CM}$) were derived. This analysis indicates that in sham animals, the TSA of fibroblasts is only about 1% that of the cardiomyocytes. Ovariectomy significantly increased $TSA_{CF/CM}$, and 17β-estradiol treatment did not alter this effect within the study time frame (Fig. 4G). Overall, these data indicate that the *uo*CBPs measured by the CaM equilibrium assay (Fig. 3) do not reflect changes in cellular compositions.

3.5. An example of changes in Ca^{2+}-dependent and Ca^{2+}-independent CaM-target interactions in LV tissues following ovariectomy and/or 17β-estradiol treatment

The data presented above indicate that the limiting CaM equilibrium in the heart, reflected by the pool of *uo*CBPs, is increased by OVX and reduced by 17β-estradiol treatment. These changes reflect combined alterations in potentially one or more of the many factors that dictate CaM-target interactions, such as total CaM-binding sites, total and free levels of CaM, affinities of target proteins for CaM, their levels of expression, Ca^{2+} sensitivities of CaM-target interactions, phosphorylation status of CaM-binding sites, among others [30]. A small fraction (estimated to be ~15 proteins [2]) of the CaM-binding network (estimated to consist of over 300 members [6]) interact with CaM in a Ca^{2+}-independent fashion [2]. As an example of how ovariectomy and/or 17β-estradiol treatment would affect target CaM interactions with endogenously saturable CaM-binding proteins (*o*CBPs), we performed coimmunoprecipitation between endogenous CaM and the inositol trisphosphate receptor (IP_3R). IP_3Rs possess separate CaM-binding sites that bind CaM in both a Ca^{2+}-dependent and Ca^{2+}-independent fashions [31,32]. We considered whether OVX and/or 17β-estradiol treatment would affect these interactions differently. Thus, coimmunoprecipitation procedures were performed with and without 1 mM $CaCl_2$ in all solutions for all steps, from tissue lysis to immunoblotting. Fig. 5A shows a representative Ponceau S stain of an SDS-PAGE membrane (upper image) and a corresponding immunoblot for total CaM (lower image) in lysates from LV tissues sham and OVX animals treated with and without 17β-estradiol. 17β-estradiol treatment increased total CaM level by approximately 20% in LV tissues from both sham and OVX animals; however, these differences were not statistically significant. Fig. 5B shows the IP_3R amounts in CaM pulldown fractions across conditions and analysis of relative Ca^{2+}-dependent IP_3R-CaM interaction. In the presence of Ca^{2+}, clear IP_3R was detected in CaM-pulldown fractions. OVX significantly reduced the amount of IP_3R associated with CaM, consistent with the increase in *uo*CBPs from our CaM equilibrium assay. 17β-estradiol treatment in sham animals reduced IP_3R-CaM interaction, also consistent with the slight increase in *uo*CBPs from the CaM equilibrium assay. However, 17β-estradiol treatment resulted in higher IP_3R-CaM association in LV tissues from OVX animals. (Fig. 5B, upper immunoblot). Interestingly, none of these changes were observed in coimmunoprecipitation experiments carried out in the absence of Ca^{2+}, despite clear association between IP_3R and CaM across treatment groups (Fig. 5B, middle immunoblot).

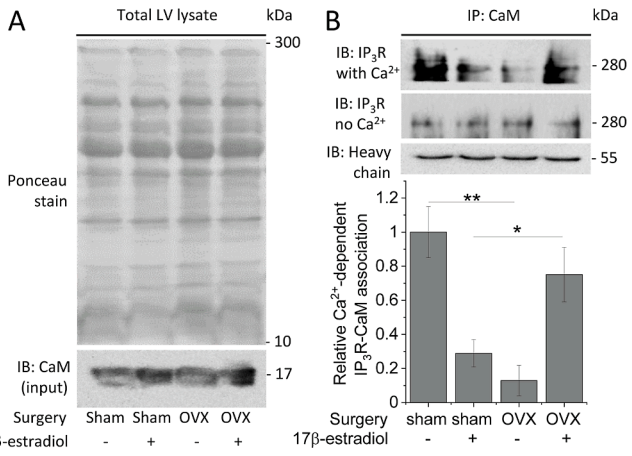

Fig. 5. Effects of experimental menopause and estrogen replacement on Ca^{2+}-dependent and Ca^{2+}-independent associations between CaM and IP_3R. Animal groups were exposed to ovariectomy and/or 17β-estradiol treatment, followed by LV tissue isolation as described in the Methods section. A) Input level of CaM. Upper, representative Ponceau S stain for SDS-PAGE membrane. Lower, total CaM expression from LV lysate. B) Pulldown fractions from LV lysates immunoprecipitated for CaM in the presence or absence of 1 mM $CaCl_2$ were immunoblotted for IP_3R in the presence (upper blot) or absence of 1 mM $CaCl_2$ (middle blot). SDS-PAGE membranes were cut between the level of IP_3R (280 kDa) and the heavy chain, followed by immunoblotting of fragments for IP_3R and IgG. Histogram, relative Ca^{2+}-dependent IP_3R-CaM association levels were obtained by correcting IP_3R immunoblotted in the presence of 1 mM $CaCl_2$ across steps for the level of total CaM expression in A. Data are means ± SD from $n = 3$ animals in each treatment group. ns, non-significant; *, $p < 0.05$; **, $p < 0.01$.

4. Discussion

The limiting nature of CaM across tissues generates a general shortage for available CaM [7–13,20], leading to a limiting CaM binding equilibrium, which is represented by the presence of CaM-binding proteins that are unoccupied by endogenous CaM (*uo*CBPs). In this work, we have devised a simple approach to assess cardiac *uo*CBPs following ovariectomy and the effects of estrogen treatment. Our LV lysate preparation protocol successfully separated CaM-binding proteins that are occupied by endogenous CaM (*o*CBPs) and those that are not (*uo*CBPs). This is indicated by the finding that flow-throughs from the mixture of LV lysate and CaM sepharose (Step 1) did not exert any effect on the binding curve between purified CaM and $BSCaM_{45}$, while equal volumes of LV eluants (Step 3) were all associated with reductions in biosensor response to the same CaM titrations.

The most striking finding using this assay is that loss of ovarian hormones exacerbates the limiting CaM equilibrium in LV tissue. Considering the complex relationships between CaM and its numerous target proteins, an increase in *uo*CBPs can indicate an increase in the expression levels of CBPs, a reduction in the expression of CaM, a reduction in interactions between CaM and CBPs, or a combination of these possibilities. Given the critical role of CaM in tissue functions, we speculate that an increase in *uo*CBPs might be associated with observed reductions in LV functions during menopause [14,15]. It is perhaps worth considering the observed effects of experimental menopause and 17β-estradiol replacement on the cardiac *uo*CBPs in the context that the G protein-coupled receptor (GPER) mediates 17β-estradiol's effect to

upregulate CaM expression in cells [16] and that GPER is regulated by Ca^{2+}-dependent interactions with CaM [19]. The exacerbated limiting CaM equilibrium in in the heart following ovariectomy might affect GPER's activity, further intensifying the effects of estrogen deprivation.

Our data demonstrate that 17β-estradiol treatment limits the increase in *uo*CBPs in LV tissues from OVX animals and abolishes the difference between LV eluants from sham and OVX animals. Interestingly, this is similar to the well-known effects of estrogen on body weight [33,34], such that 17β-estradiol prevents weight gain in both sham and ovariectomized animals (Fig. 2A). The estrogen-induced reduction in the increase in *uo*CBPs in LV tissues from OVX animals may indicate a reduction in the expression levels of CBPs or an increase in expression of CaM. It may also be caused by reductions in CaM interactions with its target proteins; however, this possibility seems less likely, as 17β-estradiol treatment in cells increases total CaM level, free Ca^{2+}-CaM concentration, and its interactions with multiple classes of CaM-binding proteins of different abundance and affinities for CaM [16]. Interestingly, the present data also indicate that use of 17β-estradiol in sham animals is associated with a slight increase in *uo*CBPs. Although this was not statistically significant, it is worth noting that 17β-estradiol treatment in sham animals may be similar to oral contraceptive use in women.

As cardiomyocytes occupy up to 80% of the volume of the rat heart [27], they are expected to contribute the most to the *uo*CBPs in our CaM equilibrium assay. Assuming an ellipsoid cellular configuration, total surface area obtained in 2-D longitudinal sections contributes two out of the three dimensions that determine a cell's volume. Our IHC analysis indicates that the 2-week's duration post-ovariectomy does not affect the TSA of the cardiomyocytes. Thus, changes in cardiomyocyte cell volume cannot explain the observed increase in *uo*CBPs caused by OVX in our CaM equilibrium assay. In OVX animals, 17β-estradiol treatment caused an increase in the TSA for cardiomyocytes, compared to both untreated OVX and sham animals. This is in line with the previous observation that 17β-estradiol induces hypertrophic growth in the murine heart [35]. However, this, again, does not explain the slight reduction in *uo*CBPs observed in the CaM equilibrium assay. Thus, changes in cardiomyocyte TSA likely are not responsible the effect of ovariectomy and 17β-estradiol treatment on the cardiac CaM equilibrium, at least for the duration investigated. Interestingly, ovariectomy increased TSA for the cardiac fibroblasts, consistent with previous observations [36]. While this is consistent with the increase in *uo*CBPs in the CaM equilibrium assay, it is highly unlikely that the change in fibroblast TSA was responsible for the change in *uo*CBPs from total LV tissue, due to their modest (~1.8%) contribution to the total heart volume [27]. Indeed, our assessment of $TSA_{CF/CM}$ indicates that the fibroblasts in LV tissue may take up only 1% surface area as do the cardiomyocytes. Whether longer 17β-estradiol treatment is required to affect the fibroblast TSA per se or relative to the cardiomyocytes ($TSA_{CF/CM}$) remains to be examined. However, these data overall suggest that the CaM equilibrium assay may provide an earlier indicator of tissue alterations in response to alterations in physiological states and/or 17β-estradiol treatment. In principle, this assay can easily be used to examine the CaM equilibrium in isolated cell cultures.

Limitation of the study: our CaM equilibrium assay only directly assesses the pool of CBPs that are unoccupied by endogenous CaM. Although the changes in *uo*CBPs result from alterations in one or more of the inputs that regulate equilibrium in the entire CaM network, they do not necessarily reflect changes in the interactions between CaM and a particular endogenously saturable CBP (*o*CBPs). Nevertheless, the example of the IP_3 receptor indicates that the behaviors of Ca^{2+}-dependent IP_3R-CaM interaction in response to ovariectomy and/or 17β-estradiol treatment are in the same trend with the findings of the CaM equilibrium assay. We do not have an explanation for the observation that Ca^{2+}-dependent IP_3R-CaM interaction is higher in LV tissues from OVX/17β-estradiol treated animals. However, ovariectomy also removes other ovarian hormones such as progesterone, which might also affect CaM-target interactions; contributions by both 17β-estradiol and progesterone to regulation of the cardiac Ca^{2+} signaling machinery have been shown [37]. It is also worth noting that our assay does not identify the proteins that constitute the pool of *uo*CBPs in each condition. Mass spectroscopy can be used subsequently should such a need present itself.

Our CaM equilibrium assay theoretically does not assess the pool of Ca^{2+}-independent CaM-binding proteins. However, with an estimate of 15 Ca^{2+}-independent CBPs [2] compared to an estimate of over 300 total CBPs [6], Ca^{2+}-independent CBPs constitute 5% or less of the entire network. In reality, some CBPs that interact with CaM in a Ca^{2+}-independent fashion also do so in Ca^{2+}-dependent manner, via the same or different binding sites [2,31,38,39]. These Ca^{2+}-independent CBPs can thus be captured by the CaM equilibrium assay in their Ca^{2+}-dependent binding mode. Therefore, this assay likely reflects changes in *uo*CBPs that result from altered binding equilibrium of over 95% of CBPs in tissues. Interestingly, our example of the IP_3R indicates that experimental menopause and/or 17β-estradiol treatment does not affect its Ca^{2+}-independent interaction with CaM.

A limitation of the study is its short time frame. While we observed significant changes in the limiting CaM equilibrium and in specific CaM-target interactions following ovariectomy and estrogen treatment, studies with longer durations may reveal novel changes in the CaM equilibrium that might reflect adaptation mechanisms to the changes in estrogen status.

5. Conclusions

We have devised a new assay that can be used to assess the status of the cardiac CaM binding equilibrium. Evaluated by this assay, removal of ovarian hormones is associated with exacerbation of the limiting CaM binding equilibrium in left ventricular tissues, an effect mitigated by early estrogen treatment (Fig. 6). The assay should also be applicable for assessing the CaM binding equilibrium in other tissues and isolated cell cultures.

CRediT authorship contribution statement

Kyle Kaster: Investigation; Formal analysis.
John Patton: Investigation; Formal analysis.
Sarah Clayton: Investigation; Funding acquisition.
Eric Wauson: Investigation; Formal analysis.
Jennifer Giles: Investigation; Visualization.
Quang-Kim Trans: Conceptualization; Funding acquisition; Supervision; Investigation; Formal analysis; Roles/Writing original and revised drafts.

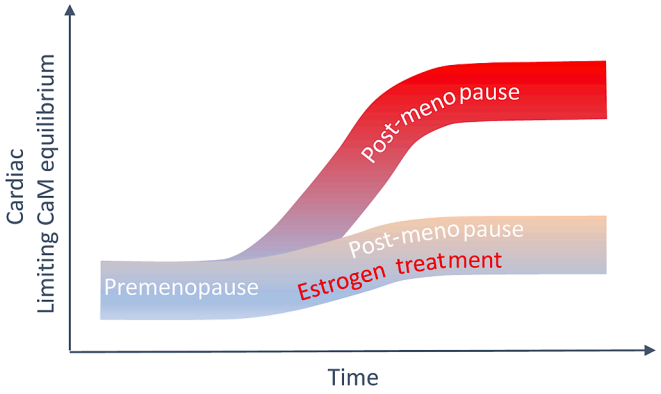

Fig. 6. Cardiac limiting CaM equilibrium and the effects of loss of ovarian hormones and estrogen treatment (see text for explanation).

Declaration of competing interest

The authors hereby attest that they have no financial or personal relationship with other people or organizations that could inappropriately influence their work presented in this manuscript.

Acknowledgments

This work was supported in part by faculty startup to SC and National Institutes of Health grant HL112184 and Iowa Osteopathic and Educational Research grant #032008 to QK-T. KK and JP were supported by Des Moines University Mentored Student Research Program (MSRP). We thank Dr. Anthony Persechini, University of Missouri-Kansas City, for the plasmid encoding $BSCaM_{45}$.

References

[1] I.B. Levitan, It is calmodulin after all! Mediator of the calcium modulation of multiple ion channels, Neuron 22 (1999) 645–648.
[2] L.A. Jurado, P.S. Chockalingam, H.W. Jarrett, Apocalmodulin, Physiol. Rev. 79 (1999) 661–682.
[3] N. Feng, M.E. Anderson, CaMKII is a nodal signal for multiple programmed cell death pathways in heart, J. Mol. Cell. Cardiol. 103 (2017) 102–109.
[4] M.J. Wleklinski, P.J. Kannankeril, B.C. Knollmann, Molecular and tissue mechanisms of catecholaminergic polymorphic ventricular tachycardia, J. Physiol. 598 (2020) 2817–2834.
[5] M. Rocchetti, L. Sala, L. Dreizehnter, L. Crotti, D. Sinnecker, M. Mura, et al., Elucidating arrhythmogenic mechanisms of long-QT syndrome CALM1-F142L mutation in patient-specific induced pluripotent stem cell-derived cardiomyocytes, Cardiovasc. Res. 113 (2017) 531–541.
[6] X. Shen, C.A. Valencia, J.W. Szostak, B. Dong, R. Liu, Scanning the human proteome for calmodulin-binding proteins, Proc. Natl. Acad. Sci. U. S. A. 102 (2005) 5969–5974.
[7] S. Kakiuchi, S. Yasuda, R. Yamazaki, Y. Teshima, K. Kanda, R. Kakiuchi, et al., Quantitative determinations of calmodulin in the supernatant and particulate fractions of mammalian tissues, J. Biochem. 92 (1982) 1041–1048.
[8] Q.K. Tran, D.J. Black, A. Persechini, Intracellular coupling via limiting calmodulin, J. Biol. Chem. 278 (2003) 24247–24250.
[9] Q.K. Tran, D.J. Black, A. Persechini, Dominant affectors in the calmodulin network shape the time courses of target responses in the cell, Cell Calcium 37 (2005) 541–553.
[10] K. Luby-Phelps, M. Hori, J.M. Phelps, D. Won, Ca(2+)-regulated dynamic compartmentalization of calmodulin in living smooth muscle cells, J. Biol. Chem. 270 (1995) 21532–21538.
[11] S.A. Kim, K.G. Heinze, M.N. Waxham, P. Schwille, Intracellular calmodulin availability accessed with two-photon cross-correlation, Proc. Natl. Acad. Sci. U. S. A. 101 (2004) 105–110.
[12] S.V. Rakhilin, P.A. Olson, A. Nishi, N.N. Starkova, A.A. Fienberg, A.C. Nairn, et al., A network of control mediated by regulator of calcium/calmodulin-dependent signaling, Science 306 (2004) 698–701.
[13] X. Wu, D.M. Bers, Free and bound intracellular calmodulin measurements in cardiac myocytes, Cell Calcium 41 (2007) 353–364.
[14] L. Groban, Q.K. Tran, C.M. Ferrario, X. Sun, C.P. Cheng, D.W. Kitzman, et al., Female heart health: is GPER the missing link? Front. Endocrinol. 10 (2020) 1–16.
[15] A.R. Sabbatini, G. Kararigas, Menopause-related estrogen decrease and the pathogenesis of HFpEF: JACC review topic of the week, J. Am. Coll. Cardiol. 75 (2020) 1074–1082.
[16] Q.K. Tran, R. Firkins, J. Giles, S. Francis, V. Matnishian, P. Tran, et al., Estrogen enhances linkage in the vascular endothelial calmodulin network via a feedforward mechanism at the G protein-coupled estrogen receptor 1, J. Biol. Chem. 291 (2016) 10805–10823.
[17] A.L. Russell, J.M. Grimes, D.O. Larco, D.F. Cruthirds, J. Westerfield, L. Wooten, et al., The interaction of dietary isoflavones and estradiol replacement on behavior and brain-derived neurotrophic factor in the ovariectomized rat, Neurosci. Lett. 640 (2017) 53–59.
[18] D.O. Larco, D.F. Cruthirds, M.J. Weiser, R.J. Handa, T.J. Wu, The effect of chronic immobilization stress on leptin signaling in the ovariectomized (OVX) rat, Endocrine 42 (2012) 717–725.
[19] Q.K. Tran, M. VerMeer, Biosensor-based approach identifies four distinct calmodulin-binding domains in the G protein-coupled estrogen receptor 1, PLoS One 9 (2014), e89669.
[20] Q. Song, J.J. Saucerman, J. Bossuyt, D.M. Bers, Differential integration of Ca2+-calmodulin signal in intact ventricular myocytes at low and high affinity Ca2+-calmodulin targets, J. Biol. Chem. 283 (2008) 31531–31540.
[21] V.A. Romoser, P.M. Hinkle, A. Persechini, Detection in living cells of Ca2+-dependent changes in the fluorescence emission of an indicator composed of two green fluorescent protein variants linked by a calmodulin-binding sequence. A new class of fluorescent indicators, J. Biol. Chem. 272 (1997) 13270–13274.
[22] A. Persechini, B. Cronk, The relationship between the free concentrations of Ca2+ and Ca2+-calmodulin in intact cells, J. Biol. Chem. 274 (1999) 6827–6830.
[23] K. Ehlers, R. Clements, M. VerMeer, J. Giles, Q.K. Tran, Novel regulations of the angiotensin II receptor type 1 by calmodulin, Biochem. Pharmacol. 152 (2018) 187–200.
[24] D.J. Black, Q.K. Tran, A. Keightley, A. Chinawalkar, C. McMullin, A. Persechini, Evaluating calmodulin-protein interactions by rapid photoactivated cross-linking in live cells metabolically labeled with photo-methionine, J. Proteome Res. 18 (2019) 3780–3791.
[25] B. Gebert-Oberle, J. Giles, S. Clayton, Q.K. Tran, Calcium/calmodulin regulates signaling at the alpha1A adrenoceptor, Eur. J. Pharmacol. 848 (2019) 70–79.
[26] A. Persechini, Monitoring the intracellular free Ca(2+)-calmodulin concentration with genetically-encoded fluorescent indicator proteins, Methods Mol. Biol. 173 (2002) 365–382.
[27] P. Anversa, G. Olivetti, M. Melissari, A.V. Loud, Stereological measurement of cellular and subcellular hypertrophy and hyperplasia in the papillary muscle of adult rat, J. Mol. Cell. Cardiol. 12 (1980) 781–795.
[28] I. Banerjee, J.W. Fuseler, R.L. Price, T.K. Borg, T.A. Baudino, Determination of cell types and numbers during cardiac development in the neonatal and adult rat and mouse, Am. J. Physiol. Heart Circ. Physiol. 293 (2007) H1883–H1891.
[29] P. Camelliti, T.K. Borg, P. Kohl, Structural and functional characterisation of cardiac fibroblasts, Cardiovasc. Res. 65 (2005) 40–51.
[30] A. Persechini, P.M. Stemmer, Calmodulin is a limiting factor in the cell, Trends Cardiovasc. Med. 12 (2002) 32–37.
[31] S. Patel, S.A. Morris, C.E. Adkins, G. O'Beirne, C.W. Taylor, Ca2+-independent inhibition of inositol trisphosphate receptors by calmodulin: redistribution of calmodulin as a possible means of regulating Ca2+ mobilization, Proc. Natl. Acad. Sci. U. S. A. 94 (1997) 11627–11632.
[32] Y. Sun, A.M. Rossi, T. Rahman, C.W. Taylor, Activation of IP3 receptors requires an endogenous 1-8-14 calmodulin-binding motif, Biochem. J. 449 (2013) 39–49.
[33] K.M. McCormick, K.L. Burns, C.M. Piccone, L.E. Gosselin, G.A. Brazeau, Effects of ovariectomy and estrogen on skeletal muscle function in growing rats, J. Muscle Res. Cell Motil. 25 (2004) 21–27.
[34] N. Yokota-Nakagi, H. Takahashi, M. Kawakami, A. Takamata, Y. Uchida, K. Morimoto, Estradiol replacement improves high-fat diet-induced obesity by suppressing the action of ghrelin in ovariectomized rats, Nutrients 12 (2020).
[35] G. Kararigas, B.T. Nguyen, L.C. Zelarayan, M. Hassenpflug, K. Toischer, H. Sanchez-Ruderisch, et al., Genetic background defines the regulation of postnatal cardiac growth by 17beta-estradiol through a beta-catenin mechanism, Endocrinology 155 (2014) 2667–2676.
[36] H. Wang, Z. Zhao, M. Lin, L. Groban, Activation of GPR30 inhibits cardiac fibroblast proliferation, Mol. Cell. Biochem. 405 (2015) 135–148.
[37] T. Bupha-Intr, J. Wattanapermpool, Regulatory role of ovarian sex hormones in calcium uptake activity of cardiac sarcoplasmic reticulum, Am. J. Physiol. Heart Circ. Physiol. 291 (2006) H1101–H1108.
[38] M. Bahler, A. Rhoads, Calmodulin signaling via the IQ motif, FEBS Lett. 513 (2002) 107–113.
[39] D.J. Black, Q.K. Tran, A. Persechini, Monitoring the total available calmodulin concentration in intact cells over the physiological range in free Ca2+, Cell Calcium 35 (2004) 415–425.